Production target and muon collection studies for an experimental muon source at CSNS

H.T. Jing [a,*], C. Meng [a], J.Y. Tang [a,c,**], B.J. Ye [b], J.L. Sun [a]

[a] Institute of High Energy Physics, CAS, Beijing 100049, PR China
[b] Department of Modern Physics, University of Science and Technology of China, Anhui 230029, PR China
[c] National Synchrotron Radiation Laboratory, University of Science and Technology of China, Anhui 230029, PR China

ARTICLE INFO

ABSTRACT

Intense muon beams have very important applications by using μSR techniques and other methods. An experimental muon source (EMuS) as a parasitic facility at China Spallation Neutron Source (CSNS) is proposed. EMuS makes use of a small portion of the high power proton beam from the CSNS accelerator complex. It will provide an excellent platform for muon beam based multidisciplinary research, and will also serve as the development base for a future full-scale muon source at CSNS. The available proton beam power of 4 kW at 1.6 GeV can produce intense muon flux with a thick production target. The muon yields with different target materials and shapes, and the muon collection efficiency have been simulated by using the FLUKA code. It is found that the graphite target of about 10–12 cm in thickness and rectangular in cross-section is a good choice, and that the collection at 90° from the beam direction is the best for surface muons. It is found that 4-D emittance volume instead of two independent 2-D emittances should be used to define the relation between the optimal muon intensity and the muon channel acceptance, due to the asymmetry between the distributions in the two transverse phase planes. The collected muon intensities for both surface muons and cloud muons with different emittances have also been studied, which are important for designing the muon beam transport line. The intensities of positive and negative muons are in the orders of $10^5\ \mu^+$/s and $10^4\ \mu^-$/s, respectively.

© 2012 Elsevier B.V. All rights reserved.

1. Introduction

With characteristics of spin and charge very sensitive to magnetic and electrical fields, short-lived subatomic muons are suitable as quantum probes of matter. The Muon Spin Relaxation, Rotation, Resonance (μSR) technique is a unique complement to other methods such as Nuclear Magnetic Resonance (NMR) and neutron scattering for the study of structure and dynamics of a material [1,2]. On the other hand, with high growth of energy consumption, the muon catalyzed fusion (μCF) will be a good direction to implement the cool fusion [3,4]. Therefore, there is an increasing demand in muon beams for studies of new materials, life science, energy resources and so on. Many laboratories around the world have proposed to construct muon facilities, although only a few are in operation due to the large budget requirement on building a high-power proton accelerator. Some details about the muon science can be found in Refs. [5–16].

China Spallation Neutron Source (CSNS) is a large scientific facility under construction, mainly for multidisciplinary research on material characterization using neutron scattering techniques [17,18]. To take the advantages of the high power proton beam delivered by the CSNS accelerators, other applications based on the proton beam including a muon source have also been proposed [19]. However, the full-scale muon source is considered to be a part of the second target station which will be constructed in the CSNS upgrading phase. In order to start research based on muon source in China as early as possible, which is hindered by the lack of muon sources at the moment, an experimental muon source (EMuS) at CSNS-I is being studied. EMuS will be driven by a 4 kW proton beam that is split from the main beam of 100 kW with a low repetition rate, say 1 Hz against 25 Hz for the main beam. As the first muon source in China it will provide a very useful tool for Chinese researchers. As for the full-scale muon source in the further future, it will be comparable to the muon sources at ISIS [7] and J-PARC [20]. The schematic layout of the CSNS including the muon sources is depicted in Fig. 1.

2. Muon generation processes

Although muons can be produced by the interaction between high-energy cosmic rays and air molecules in the atmosphere, they are too kinetic and the intensity is too weak. Usually,

* Corresponding author. Tel.: +86 1088233992.
** Corresponding author at: Institute of High Energy Physics, CAS, Beijing 100049, PR China. Tel.: +86 1088233992.
E-mail addresses: jinght@ihep.ac.cn (H.T. Jing), tangjy@ihep.ac.cn (J.Y. Tang).
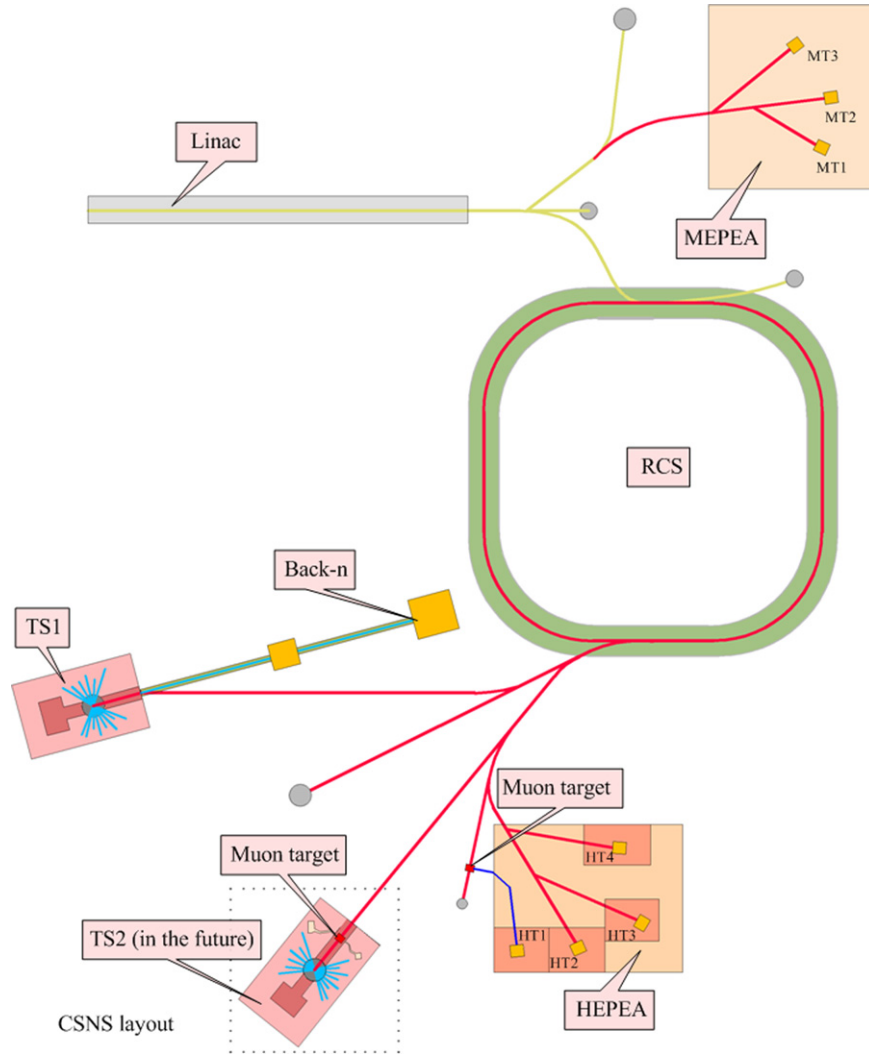
Fig. 1. Schematic of CSNS layout. The high and medium energy proton experimental areas (HEPEA and MEPEA) are arranged at CSNS. 2nd Target Station (TS2) is to be built in the upgrading phase.

researchers prefer artificial muon beams by using high-intensity and medium-high energy proton beams to bombard targets. There exists an intermediate process that the nucleon–nucleon interactions from the bombardment of protons on target produce pions. Pions then decay into muons. Therefore, the muon yield will be mainly determined by the corresponding pion yield. The elementary production mechanisms of pions are dominated by the single and double pion production processes, as depicted below.

Single pion production process

$$\left. \begin{array}{l} p+p \rightarrow p+n+\pi^+ \\ p+n \rightarrow p+p+\pi^- \\ p+n \rightarrow n+n+\pi^+ \\ p+p \rightarrow d+\pi^+ \end{array} \right\}$$

Double pion production process

$$\left. \begin{array}{l} p+p \rightarrow p+p+\pi^+ +\pi^- \\ p+p \rightarrow n+p+\pi^+ +\pi^0 \\ p+p \rightarrow d+\pi^+ +\pi^0 \end{array} \right\} \text{ and } \left. \begin{array}{l} p+n \rightarrow p+n+\pi^+ +\pi^- \\ p+n \rightarrow n+n+\pi^+ +\pi^0 \\ p+n \rightarrow p+p+\pi^- +\pi^0 \\ p+n \rightarrow d+\pi^+ +\pi^- \end{array} \right\}$$
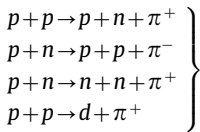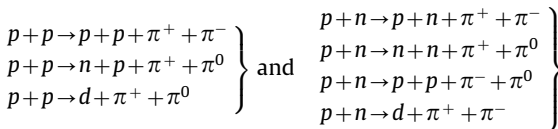
Muons are generated in the decay processes of positive and negative pions [21]

$$\left. \begin{array}{l} \pi^+ \xrightarrow{26.03 \text{ ns}} \mu^+ +\upsilon_\mu \\ \pi^- \xrightarrow{26.03 \text{ ns}} \mu^- +\bar{\upsilon}_\mu \end{array} \right\} \cdots 99.988\%$$
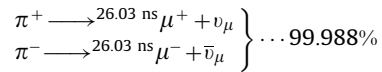
The proton beam energy of 1.6 GeV at CSNS is near the peak energies in the pion production spectra of both three-body final states and four-body final states, and thus very suitable for muon production.

3. Simulation studies on the muon production target and the muon collection at EMuS

The characteristics of target material, size and shape are extremely important for the production and collection of muons. Therefore, the production and transport of pions and muons in target have been simulated by using FLUKA [22,23], a widely used code based on the Monte Carlo method. The latest version of FLUKA 2011.2 can simulate muon production processes from low energy to high energy by employing the scattering data library and the theoretical model.

The size of the proton beam spot at target is a very important factor to determine the target dimensions. This is due to the short stopping ranges of low energy pions and muons. From the RTBT (Ring-to-Target-Beam-Transport) beam optics studies, where a dual-Gaussian distribution each truncated to $\pm 3\sigma$ with the beam core emittances of 80π mm mrad and the beam halo emittance of 250π mm mrad is assumed [24], one can design a beam spot at the muon target as small as possible in the beam transport line of hosting the muon target. The following expression of the beam spot distribution at the muon target is used for the studies:

$$f(x,y) = 0.97 f_1(x,y) + 0.03 f_2(x,y)$$
$$f_1(x,y) = \frac{1}{2\pi\,\sigma_{x1}\,\sigma_{y1}} \exp\left(-\frac{1}{2}\left(\frac{x}{\sigma_{x1}}\right)^2 - \frac{1}{2}\left(\frac{y}{\sigma_{y1}}\right)^2\right), \quad |x| \le 3\sigma_{x1}, \quad |y| \le 3\sigma_{y1}$$
$$f_2(x,y) = \frac{1}{2\pi\,\sigma_{x2}\,\sigma_{y2}} \exp\left(-\frac{1}{2}\left(\frac{x}{\sigma_{x2}}\right)^2 - \frac{1}{2}\left(\frac{y}{\sigma_{y2}}\right)^2\right), \quad |x| \le 3\sigma_{x2}, \quad |y| \le 3\sigma_{y2}$$

$$(1)$$

Where $\sigma_{x1} = \sigma_{y1} = 5.777$ mm and $\sigma_{x2} = \sigma_{y2} = 7.077$ mm. The distribution is shown in Fig. 2.

For those kinetic pions that can escape from the target, they will quickly decay into muons in flight. The so-called decay muons can be collected in a superconducting solenoid to form a muon beam and be transported to experimental endstations. For those low-energy pions that cannot escape from the target, they will decay into muons where they are stopped. The muons from the stopping pions on the target surface can emit out and be collected as surface muons. However, only the positive muons can emit out from the target, because the stopping negative pions will be immediately captured by target nuclei to form 'pionic stars' [5]. Compared with decay muons, surface muons have the advantages of high intensity and 100% polarization. In addition, the average energy of a surface muon beam is low and it does not need a costly superconducting solenoid as needed for decay muons. This will result in a low budget requirement for the muon beam transport line. For the EMuS, it is designed to focus on surface muons, but the so-called cloud muons which pions decay in flight in a region close to the target are also incorporated into consideration. In this paper, we will mainly focus on the target design that is optimized for the production of surface muons and also on the collection of surface muons and cloud muons.

3.1. Target materials for producing muons

To obtain high-flux muons, one needs a high-intensity and high-energy proton beam. For the target material, it should have a good thermal conductivity to remove the high heat deposit in target and a good muon production rate. Usually a trade-off is needed between the two properties. Here several materials which are usually used in many laboratories have been compared. A quadrate target with dimensions of $20(W) \times 15(H) \times 15$ cm^3(L) and a dual-Gaussian beam spot as shown in Fig. 2 are used to calculate the total yield of surface muons.

The center of beam spot is at the origin, and different target positions are used to study the effect of different impact depths. A muon collector with a round aperture of 135 mm is placed at $90°$ (lateral side) with respect to the proton beam at 60 cm from the target. The collector can be considered as the entrance of the muon beam transport line (MBT), but the aperture used here is only for the comparison study. The practical entrance aperture of the MBT will be determined by the MBT acceptance, and the vacuum aperture varies along the MBT.

In general, the cross-section of pion production induced by proton is larger for nucleus with larger mass number [25]. For a single-element material, the muon production is determined by the atomic number and the material density of the element. However, the larger the material densities are, the shorter the projection ranges of pions and muons are. One can find that the obtained surface muon intensities from the different materials are not very different as shown in Fig. 3, with copper slightly better.

It is also possible to collect the surface muons which emit from the target front surface in the forward direction or with a small angle to the proton beam axis. In Fig. 4, the yields of surface muons emitted from the front surface of a quadrate target for different materials are shown. The width and height of the target are $15(W) \times 15$ cm^2(H). The center of the target width is aligned with the beam axis. However, except for the first 20–30 mm, increasing the target lengths has quite limited gain to the yields. It is found that the surface muon yield from the front surface is lower than that from the lateral surface in the case of a thick target. However, for higher-energy muons it is preferred to collect them in the forward direction or with a small angle to the proton beam axis because of the forward effect of kinetic pions.
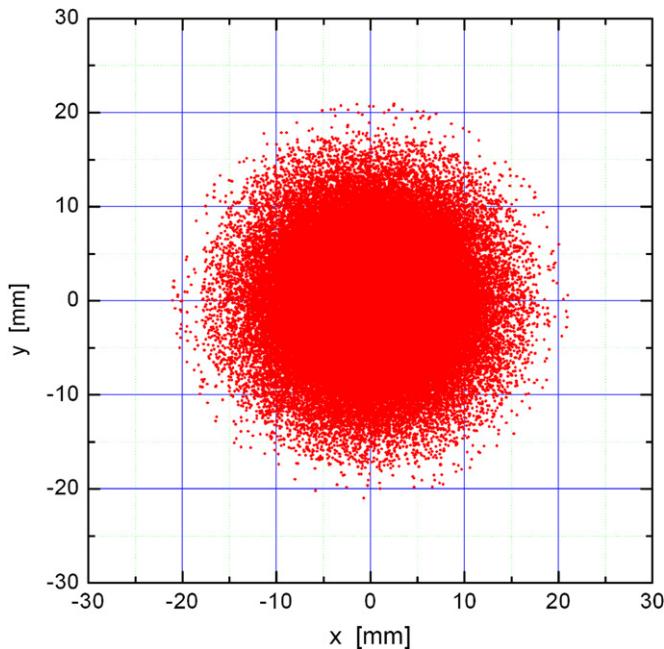
Fig. 2. Distribution of the proton beam spot at the muon target, which is a dual-Gaussian distribution each truncated to $\pm 3\sigma$.
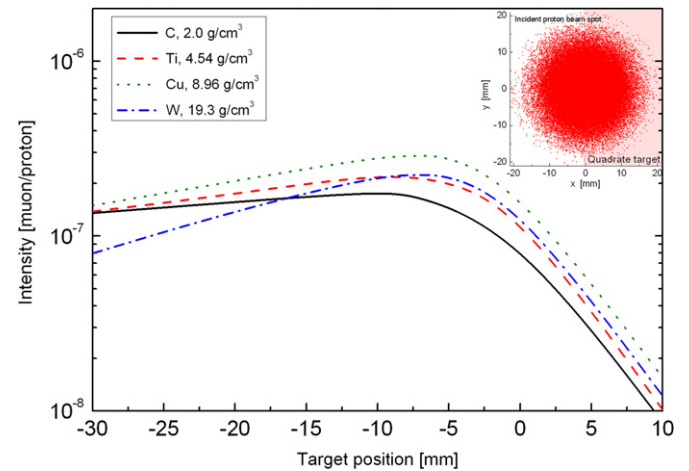
Fig. 3. Surface muon yields for different target materials from a collector at 60 cm from the left lateral side of target vs. positions of the left edge of target relative to the beam axis. The beam spot on the front surface of target is also shown in the upper-right corner.
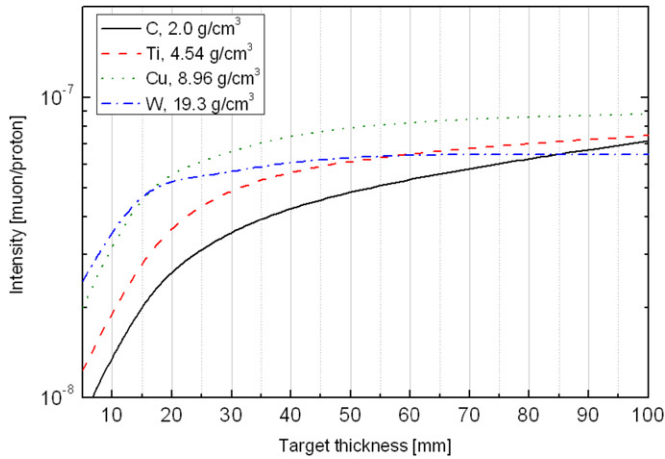
Fig. 4. Yields of surface muons from a collector at 60 cm from the front surface of a quadrate target of different materials vs. the target lengths.

For example, the pions and decay muons from the front surface are utilized at the KEK UT-MSL BOOM facility [26].

For a target material with larger mass number, the muon and neutron yields will increase simultaneously. A large amount of neutrons will result in a large local radiation dose rate and increase the difficulties for radiation shielding. As a compromise, a carbon target is preferred for EMuS. However, we will also keep the possibility of using other target materials.

3.2. Different target shapes

Almost all muon sources have been constructed together with spallation neutron sources or other facilities by employing high power proton beams. The sharing of proton beam saves the costs of constructing very costly high-power proton accelerators. Two modes can be employed to utilize proton beam to produce muons, namely the mainstream mode and the part-time mode. The first mode is used by most of the existing muon sources such as the ones at PSI, ISIS, TRIUMF, J-PARC and so on. The targets are penetrable or relatively thin so that the main beam power can be used for other applications. The surface muons and kinetic muons can be collected in the front and/or in the back at an angle with respect to primary proton beam. As mentioned in Ref. [13], thicker targets would increase the muon flux but the target thickness should be a compromise between the use of the muon channel and other mainstream beam applications, as the muon production target not only consumes the proton beam by nuclear reactions but also deteriorates the proton beam quality with multiple scattering effects. Therefore, a muon source with a thin target is usually designed to consume about 5% of the total proton beam power. The second mode is usually used by some small muon sources such as the ones at LBL, AGS, KEK and so on. Only a relatively small portion of the main proton beam is extracted and transported to the muon production area. After the proton beam penetrates the muon target, it goes into a beam dump directly. Thick targets are preferable for these small muon sources. This is just the case for EMuS.

Before we study the surface muon yields for different target shapes, it is necessary to know about the surface muon characteristics. Because a number of stopping positive pions swarm the target surface layer, the surface muons may emit from the target skin isotropically. The most important factor affecting the yield of surface muons is their paths to the surface in the target skin because of the short stopping range. Obviously, the surface muons have higher probabilities to escape from the target along the direction normal to the surface. We employ a carbon target

with dimensions of $3(W) \times 15(H) \times 15\ cm^3(L)$ to calculate the surface muon yields from a lateral surface. From Fig. 5, one can find that the surface muon flux at the normal direction of target skin are the highest and decreases with angle by approximately following the law of $I \propto \cos(\theta - 90°)$ [16].
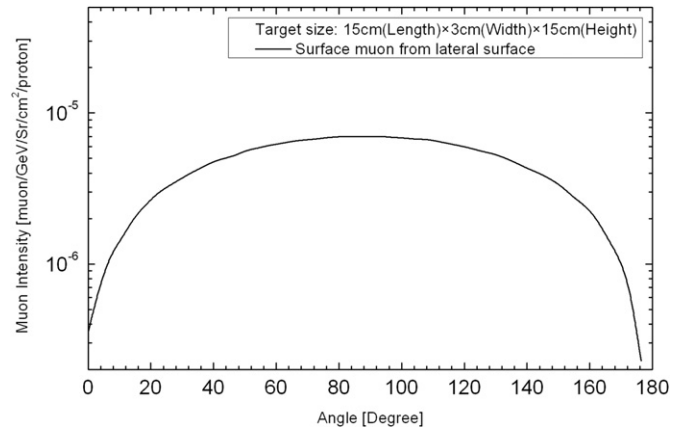
Fig. 5. Surface muon yields versus muon emission angles with respect to the incident proton beam direction.
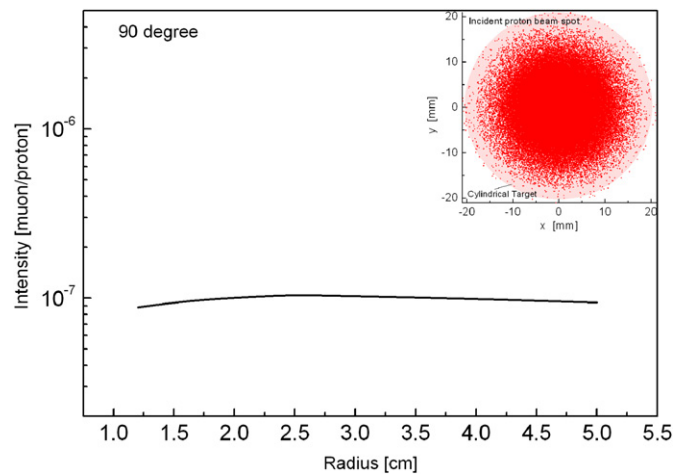
Fig. 6. Surface muon intensity as a function of radius for a cylindrical carbon target. The beam spot on the front surface of the target is also shown in the upper-right corner.
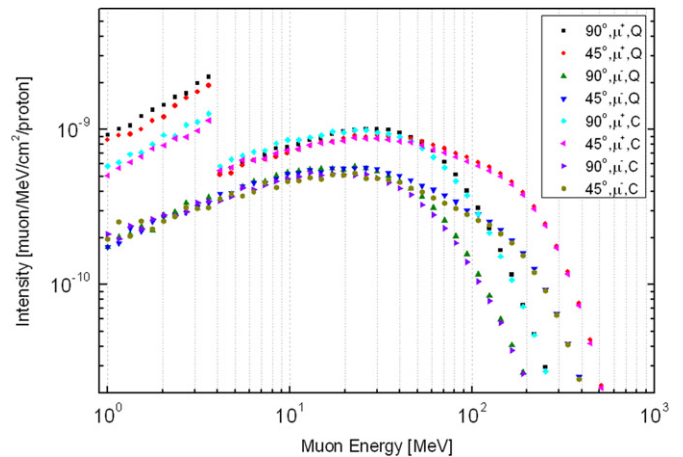
Fig. 7. Energy spectra for the positive and negative muons from the cylindrical (C) and quadrate (Q) carbon targets with the collectors at the emission angles of 45° and 90°.

A cylindrical target is also studied to be compared with the quadrate target as shown in Fig. 3. The surface muon yields for different target radii are shown in Fig. 6. The lateral collector is also at 60 cm from the target surface. One can find that the optimal radius is about 2.5 cm for the given proton beam distribution, but the change in yield is quite small for different radii. The energy spectra for the two target shapes are shown in Fig. 7. It is evident that a quadrate target is favored not only for its higher muon collection efficiency but also for its good mechanical properties facilitating water-cooling and support designs. Fig. 7 also reveals an interesting property: for kinetic or decay muons, either positive or negative, the collection at 45° is favored.

4. Muon intensity and acceptance of the muon beam transport line

For the design of a muon source, the most important is to deliver as many muons as possible to experimental stations. This means that the muon production yield, the collection efficiency and the transport efficiency are all important. On the one hand, the muon production yield is limited mainly by the proton beam intensity; on the other hand, the collection and transport efficiency are limited by the acceptance of the muon beam transport line (abbreviated as MBT). Larger acceptance means higher cost of the transport line, and also larger muon beam spot at the experimental sample that sometimes one does not desire. Therefore, a very long target is not favorable because the collection efficiency for the muons emitted from the target surface area outside the projection of the collector aperture is very low. For quantitive analysis, the distributions in phase spaces and the optical transfer to the collector have been studied to determine the relation between the collection efficiency and the acceptance. With a quadrate carbon target with dimensions of $15(L) \times 3(W) \times 5$ cm^3(H), the aperture of the collector (or the MBT entrance) of 135 mm and the distance of 60 cm between the target surface and the collector, the surface muon distributions in the transverse phase planes are given in Fig. 8. Here the muon energy is limited from 3.56 MeV to 4.15 MeV, corresponding to the central energy of 3.86 MeV and the energy spread of $\pm 7.5\%$ or the momentum spread of $\pm 3.83\%$. One can find the two distributions are quite different: the one in the horizontal plane is more uniform in the center and has larger emittance for a given beam fraction; the one in the vertical plane has more trace of the initial proton beam distribution.

Before carrying out the optics design of the MBT, one needs to determine the acceptance of the beam line and the Courant–Snyder parameters (or C–S parameters) at the entrance. The acceptance

is a trade-off between the construction/operation cost of the beam line and the muon intensity at the endstation, with larger acceptance for higher intensity. The C–S parameters are important for designing the MBT optics, and they should be adopted according to the muon distribution in the phase space at the MBT entrance that is defined as the collector described above. Otherwise, for the same acceptance fewer muons will be transported. It is found that with this special muon distribution one needs to adopt 4-D phase space description instead of two independent transverse phase planes in usual cases, if one wants to obtain the optimum muon intensity with a given sum of the emittances in the two transverse phases. The main reasons are that the muon distributions in the two transverse phase planes are different and that the muon beam emittances have to be limited according to the MBT acceptances. Once the 4-D acceptance is obtained with the given beam fraction or muon intensity, the acceptances in the two projection phase planes can be easily derived.

For a decoupled 4-D ellipsoidal phase space, its volume can be expressed by the product of the projected emittances in $x - x'$ and $y - y'$

$$V = \frac{1}{2}\pi^2 \varepsilon_x \varepsilon_y \tag{2}$$

The emittances ε_x and ε_y can be expressed by two ellipse equations

$$\begin{cases} \varepsilon_x = \gamma_x x^2 + 2\alpha_x x x' + \beta_x x'^2 \\ \varepsilon_y = \gamma_y y^2 + 2\alpha_y y y' + \beta_y y'^2 \end{cases} \tag{3}$$

where (γ_x, α_x and β_x) and (γ_y, α_y and β_y) are the C–S parameters in the $x - x'$ and $y - y'$ phase planes, respectively.

First, one calculates the particle density distribution in the 4-D phase space. Next, one can fit 4-D density contours with the C–S parameters (α_x, β_x, α_y and β_y) for different beam fractions. Finally, the 4-D ellipsoid volume and the two projection emittances for different contours or beam fractions can be obtained. To obtain the density contours and the C–S parameters for different contours, the Courant–Snyder invariant density emittance analysis method [27] has been applied. This method uses the neighboring particles within a small ellipse centered at the certain particle to mark the local C–S invariant density. Then the C–S invariant density distribution as shown in Fig. 8 can be used to define the density contours representing the beam fractions that they encircle. For different beam fractions or emittances, the C–S parameters are also different as the inner and outer contours of the muon distribution are not exactly similar in shape.
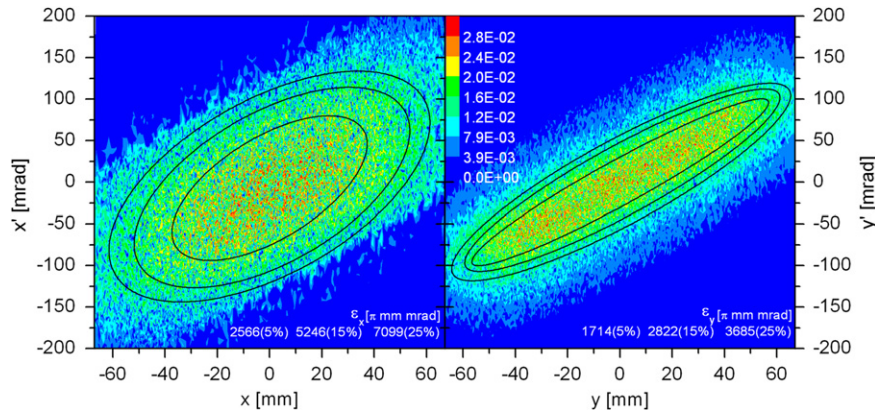
Fig. 8. Density distributions of surface muons in $x - x'$ and $y - y'$ phase planes. The emittance ellipses from small to big are the projections of the 4-D ellipsoids, and they represent the beam fractions of total recorded particles: 5%, 15% and 25%.

Fig. 9 shows the surface muon intensities vs. 4-D ellipsoid volumes. The simulations show that one can achieve the prospective design goal of 10^5 μ^+/s if the 4-D ellipsoid volume in the transverse phase space is larger than $2.2 \times 10^6 (\pi$ mm mrad$)^2$, corresponding to 2566π mm mrad in $x-x'$ and 1714π mm mrad in $y-y'$. Obviously, one can obtain higher muon intensity by increasing the emittances considerably, as shown in Table 1. One can find that the C–S parameters change with the beam fractions, especially in the phase plane $y-y'$. On the other hand, for smaller acceptance of MBT, a relatively shorter muon target can be used as the two ends of the target contribute very little in this case, as shown in Fig. 10.

5. Intensities of cloud muons

Besides stressing on the exploitation of surface muons at EMuS, it is also hoped to exploit higher-energy muons that have also sizable intensity despite lower than that of surface muons. As mentioned in Ref. [6], cloud muons are one kind of decay muons which pions decay in flight in a region close to the production target. It is possible to utilize cloud muons by just adjusting the optical parameters of the MBT. Both positive and negative cloud muons can be available. In Fig. 7, one can find that the intensities of cloud muons are about one order lower than that of surface muons, but one can use a wider momentum bite, for example, $\Delta p/p \approx \pm 5.0\%$. The collection geometry is the same as that for surface muons, but the MBT should be designed with

higher magnetic rigidity for transporting more kinetic cloud muons. Same as for surface muons, the 4-D-ellipsoid density analysis method is still employed to analyze the beam distribution of cloud muons in the transverse phase space and obtain the relation between the cloud muon intensities and the 4-D-ellipsoid volumes.

In order to obtain the cloud muon intensities as high as possible, the energies of the cloud muons are centered at the peaks of energy spectra as shown in Fig. 7, namely 27.5 MeV and 20 MeV for positive and negative muons, respectively. The phase-space density distributions of cloud muons are very similar to those of surface muons. The intensities vs. 4-D ellipsoid volumes for cloud muons are shown in Fig. 11, and the C–S parameters for some typical cases are listed in Table 1. With the same 4-D ellipsoidal volume of $2.2 \times 10^6 \pi^2$ mm^2 mrad^2, the intensities of positive and negative muons can exceed 10^5 μ^+/s and 10^4 μ^-/s, respectively, which are excellent for such an experimental muon source.

6. Time structure of the muon beams

The CSNS accelerator is designed to deliver a proton beam with energy of 1.6 GeV and a pulse repetition rate of 25 Hz to a tungsten target. For EMuS, the proton beam with only one pulse per second or 1 Hz in repetition rate is directed to the muon production target. For a pulsed muon source, there exist great advantages as remarked by Eaton [5]: (1) the μSR experiments

Fig. 9. Surface muon intensity vs. 4-D ellipsoid volume.
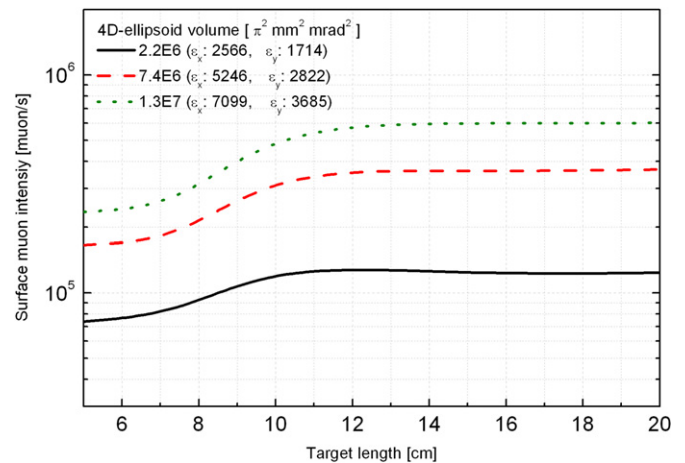
Fig. 10. Surface muon intensities vs. target lengths for three typical 4-D ellipsoid volumes.

Table 1
The optimal combinations of partial $x-x'$ and $y-y'$ emittances and the corresponding C–S parameters at the MBT entrance for given 4-D ellipsoid volumes or muon intensities.

	ε_x (π mm mrad)	α_x	β_x (m)	ε_y (π mm mrad)	α_y	β_y (m)	4-D vol (π^2 mm^2 mrad^2)	Intensity (μ/s)
Surface muons	7099	−0.663	0.531	3685	−1.835	1.140	1.3E+07	6.0E+05
	5246	−0.682	0.530	2822	−2.120	1.288	7.4E+06	3.6E+05
	2566	−0.772	0.542	1714	−3.165	1.878	2.2E+06	1.2E+05
Cloud positive muons	7544	−0.553	0.438	3451	−1.804	1.146	1.3E+07	1.4E+06
	5580	−0.601	0.446	2651	−2.019	1.266	7.4E+06	8.4E+05
	2734	−0.686	0.476	1603	−2.934	1.790	2.2E+06	2.9E+05
Cloud negative muons	7509	−0.577	0.444	3495	−1.880	1.185	1.3E+07	4.9E+05
	5655	−0.577	0.444	2632	−1.880	1.185	7.4E+06	2.9E+05
	2905	−0.655	0.482	1526	−2.563	1.594	2.2E+06	9.9E+04

Notation: for surface muons, $E_{ave} = 3.86$ MeV, $\Delta p/p \approx \pm 3.83\%$; for cloud positive muons, $E_{ave} = 27.5$ MeV, $\Delta p/p \approx \pm 5\%$; for cloud negative muons and $E_{ave} = 20$ MeV, $\Delta p/p \approx \pm 5\%$.

with pulsed sources are in general much faster than conventional time differential ones on continuous sources by using the segmentation of the detectors to count the muon decays; and (2) the muons in former pulses will decay completely in the sample without interfering the next muon pulse. This means that the background for experiments is very low so that muon decays in the sample can be traced over many muon lifetimes. Furthermore, some muon science experiments are particularly suited to pulsed sources including radio-frequency techniques with muons, muon

catalyzed nuclear fusion, fundamental physics studies with muonium using pulsed lasers and studies in material science using ultra slow muons. As a pulsed muon source, the time structure of the muon beams at EMuS needs to be investigated, which leads to an upper limit on precession frequencies which can be measured [28]. Usually, a general requirement of the μSR technique is that the pulse width of muon beam must be considerably shorter than the muon lifetime, while the pulse repetition period must be longer than the muon lifetime [29].

There are three important factors determining the time structure of the muon beam at the collector: the first one is the pulse width of the proton beam; the second one is the time spread due to pion decay; and the third one comes from the momentum spread of muons. The simulations by FLUKA can give the time spread at the collector including the last two factors and also other weak influence factors, and then one can use the convolution of the function of the proton pulse and the time spread at the collector to obtain the total time structure of the muon beam. The CSNS accelerator supplies proton pulses with two bunches in train; each is assumed to be parabolic in shape with a total length of 70 ns and separated by about 400 ns. For more details about the proton time structure and the convolution method, one can refer to Ref. [30]. The total time structures for the surface muons and cloud muons are shown in Fig. 12. If needed, the two bunches in a pulse can be split into two sub-muon channels by using a fast kicker in the MBT as commonly used in other muon sources. The debunching effect along with the MBT has also been studied. Despite the momentum spread being very large, its contribution to the time spread at the endstation of about 30 m is negligible compared with the initial proton bunch width, mainly due to relatively large beam velocity.
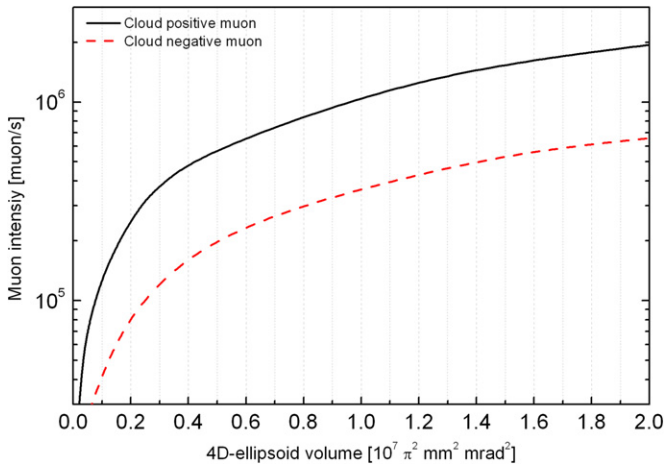
Fig. 11. Cloud muon intensities vs. 4-D ellipsoid volumes for both positive and negative muons.
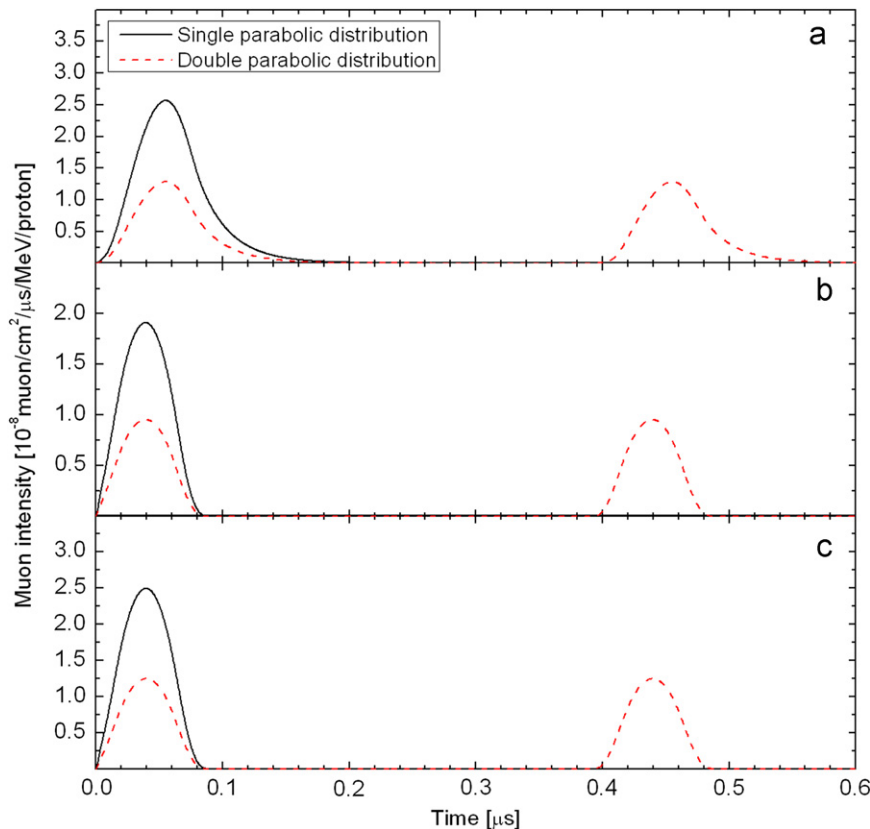
Fig. 12. Muon pulse shapes for different energies at the 90° collector at 60 cm from the target. The solid and dashed lines denote the cases with a single-parabolic distribution (one bunch per pulse) and a double-parabolic distribution (two bunches per pulse) for the proton beam, respectively. (a) Surface moun 3.56Mev~4.15Mev, (b) Cloud position moun 25.0Mev~30.0Mev, (c) Cloud negative moun 18.2Mev~21.8Mev

7. Conclusions

The muon yield's dependence on the material and the shape of the muon production target at EMuS has been investigated. It is found advantageous to collect surface muons at the lateral side from a thick quadrate target. For the special distribution of the surface and cloud muons, 4-D ellipsoid emittance is used to determine the relation between the intensity of the collected muons and the acceptance of the muon beam transport line. At the same time, for the most efficient transport of the muon beams, one also needs to design the MBT with an asymmetric transverse acceptance with the horizontal one being larger. For the proton beam of 4 kW in beam power at EMuS, one can expect to obtain the intensities of surface and cloud muons in the order of $10^5 \, \mu^+/s$, with a modest sum acceptance of about 4500π mm mrad of the MBT.

The beam optics design of the MBT together with the design of the experimental endstations will be carried out in the future. As the first muon source in China, we hope that EMuS can provide muon beam for experiments together with the completion of the CSNS in 2017.

Acknowledgments

References

[1] J. Major, et al., Zeitschrift fur Physik C 56 (1992) S269.
[2] R.D. Renzi, NMR, μSR and Mössbauer Spectroscopies in Molecular Magnets, Springer Milan, 2007, p. 149.
[3] L.I. Ponomarev, Contemporary Physics 31 (1990) 219.
[4] W.H. Breunlich, et al., Annual Review of Nuclear and Particle Science 39 (1989) 311.
[5] G.H. Eaton, RAL Technical Reports, RAL-TR-98-019,1998.
[6] G.M. Marshall, Zeitschrift fur Physik C 56 (1992) S226.
[7] G.H. Eaton, Zeitschrift fur Physik C 56 (1992) S232. RAL Report, RAL-TR-98-019, 17–28 August 1998.
[8] Y. Matsuda, et al., AIP Conference Proceedings 721 (2004) 313.
[9] G. Heidenreich, AIP Conference Proceedings 642 (2002) 122.
[10] K. Nagamine, Hyperfine Interactions 8 (1981) 787.
[11] Y Miyake, et al., Journal of Nuclear Materials 343 (2005) 21.
[12] W.J. Kossle, Hyperfine Interactions 8 (1981) 797.
[13] P.A. Thompson, et al., Nuclear Instruments and Methods in Physics Research 161 (1979) 391.
[14] F. Foroughi, et al., Hyperfine Interactions 138 (2001) 483.
[15] M.K. Craddock, et al., Nature 270 (1977) 671.
[16] A.E. Pifer, et al., Nuclear Instruments and Methods in Physics Research 135 (1976) 39.
[17] S.X. Fang, et al., Journal of the Korean Physical Society 48 (2006) 697.
[18] J. Wei, et al., Journal of the Korean Physical Society 50 (2007) 1377.
[19] J.Y. Tang, et al., Chinese Physics C34 (2010) 121.
[20] Y. Miyake, et al., Physica B326 (2003) 255.
[21] Particle Data Group, Physics Letters B 591 (2004) 1.
[22] A. Ferrari, P.R. Sala, A. Fassò, J. Ranft,FLUKA: a multi-particle transport code, CERN 2005–2010, INFN/TC-05/11, SLAC-R-773, 2005.
[23] G. Battistoni, S. Muraro, P.R. Sala, F. Cerutti, A. Ferrari, S. Roesler, A. Fassò, J. Ranft, The FLUKA code: description and benchmarking, in: M. Albrow, R. Raja (Eds.), Proceedings of the Hadronic Shower Simulation Workshop 2006, Fermilab, 6–8 September, 2006, AIP Conference Proceeding 896 (2007) 31–49.
[24] J.Y. Tang, et al., Nuclear Instruments and Methods in Physics Research A582 (2007) 326.
[25] J.F. Crawford, et al., Physical Review C22 (1980) 1184.
[26] K. Nagamine, UT-MSL Newsletter 5 (1985) 3.
[27] J.L. Sun, et al., Chinese Physics C 35 (2011) 1.
[28] S.J. Blundell, Contemporary Physics 40 (1999) 175.
[29] Jeff E. Sonier, A brochure of Muon Spin Rotation/Relaxation/Resonance (μSR) Technique. 〈www.chem.ubc.ca/research/muSRBrochureFinal_April11.pdf〉.
[30] H.T. Jing, et al., Nuclear Instruments and Methods in Physics Research A621 (2010) 91.